Development of non-covalent triazine framework decorated carbon nanotube as a photocatalyst support for methylene blue dye degradation

Setty Ratnakumari
Jawaharlal Nehru Technological University Kakinada
Dakshinamoorthy Prasanna
Vignan's Nirula Institute of Technology and Science for Women
Vejendla Anuradha
anuradha@vignandegreecollege.ac.in

Jawaharlal Nehru Technological University Kakinada
T. Raja Rajeswari
Sri A.S.N.M Government College

Research Article

Keywords: Triazine, Methylene blue, Zinc sulfide-tin sulfide, carbon nanotube, photocatalyst

Posted Date: June 26th, 2023

DOI: https://doi.org/10.21203/rs.3.rs-3044194/v1

Additional Declarations: No competing interests reported.

Abstract

Non-covalent triazine framework decorated carbon nanotube were prepared by using cyanuric chloride (CC) and biphenyl (BP) and carbon nanotube (CNT) by Friedel-Crafts reaction. The prepared poly(cyanuric chloride-*co*-biphenyl)-carbon nanotube (Poly(CC-*co*-BP)-CNT) composite is used as a supporting materials for photocatalyst towards methylene blue (MB) dye degradation. Zinc sulphide (ZnS) and Zinc sulphide-Tin sulphide (ZnS-SnS) nanoparticles were doped on the surface of poly(cyanuric chloride-*co*-biphenyl)-carbon nanotube (Poly(CC-*co*-BP)-CNT) composite by using aqueous plant extract of *Vanda Testacea* as reducing agent. The ZnS/Poly(CC-*co*-BP)-CNT and ZnS-SnS/Poly(CC-*co*-BP)-CNT photocatalyst were analyzed using UV-DRS, PL, XRD, EDX and TEM methods. The durability of the prepared photocatalyst were tested using methylene blue dye under different UV light sources and sun light. The photocatalytic activity of ZnS-SnS/Poly(CC-*co*-BP)-CNT photocatalyst is found to be higher than ZnS/Poly(CC-*co*-BP)-CNT, unsupported ZnS and ZnS-SnS photocatalyst towards MB dye. This confirms that prepared ZnS-SnS/Poly(CC-*co*-BP)-CNT photocatalyst is effective for the removal of the methylene blue dye from waste water.

1. INTRODUCTION

Most threatening environmental pollution is water pollution. The major source for water pollution is industrial effluents, which gives carcinogenic effects to human beings, aquatic animals and environment. Industrial effluents like reactive dyes were utilized more in the textile, cosmetic, pharmaceutical, fabric and plastic industries [1, 2]. Water soluble dyes will seriously affect the human health which causes pulmonary congestion liver damage, vomiting, diarrhea [3, 4]. In this point of view the removal of reactive dyes is found to be very essential from the industrial effluents, these industrial effluents were reported to be treated by several physiochemical methods like trickling filters [5] activated sludge [6], microfiltration [7], adsorption [8], chemical coagulation [9], reverse osmosis [10], photocatalytic degradation [11–14] for decolorization/decomposition/degradation of dye molecules. Among physiochemical methods, photocatalytic degradation is a sustainable method because the renewable solar energy is utilized for dye degradation which converts the hazardous organic pollutants and microorganisms into harmless substances like H_2O and CO_2. [15–17].

Generally, dye degradation takes place through the photochemical reaction. The effective dye degradation process is limited by the recombination rate of the photo-generated electron-hole pairs formed during the photocatalytic process and unsuitable interfacial charge-transfer process of photogenerated charge carriers. Thus, development of photochemically active heterogeneous photocatalyst of non-precious metal oxides/sulfide [18–23] is a major challenge for the researchers. This limitation can be overcome by coupling of two different semiconductor of metal oxide/sulfide. The coupled metal oxide/sulfide semiconductor (i) that reduces the electron-hole pairs recombination process and (ii) the proper spatial structure for separation of electron and hole pairs which gives enhanced photocatalytic activity. Recently, the development of semiconducting materials from II-VI group elements in the periodic table has attracted attention due to their low band gap under Ultra-Violet

and solar light irradiation. According to previous report semiconducting materials like Ag_2S [24], PbS [25, 26], CdSe [27, 28], CuS [29, 30], CdS [31, 32], MoS_2 [33, 34], SnS_2 [35, 36], ZnS [37, 38] are active towards dye degradation under solar and ultraviolet light. Among them ZnS is a chalcogenide semiconductor with a moderate band gap values ~3.72 eV at room temperature [39] and it is most widely studied material because of low cost, non-toxicity and Ultra-Violet active photocatalyst towards dye degradation. Apart from the dye degradation, the ZnS is broadly used in various fields such as light emitting diode (LED), flat panel display lasers, electroluminescence, biodevices, electro-optic modulator, infrared windows, optical sensors, phosphors, photoconductors etc, [40–48]. The ZnS nanostructure were prepared by chemical methods like hydrothermal [49], co-precipitation [50], polyol [51], nonaqueous chem{ical [52], microwave-solvothermal [53] and chemical bath deposition [54]. Now-a-days, the preparation of metal sulphides by biological methods has acquired greater significance because of its eco-friendliness, simplicity and controlled chemical toxicity towards environment.

Vanda Testacea is a species of *vandaceous orchid* originated in Indian subcontinent to Indochina *and it* is broadly used for its medicinal properties. The roots, leaves and flowers of *Vanda Testacea* are utilized as herbal medicines for remedy of nervous disorders, anti-cancerous drug, inflammations, rheumatism, piles, bronchitis [55]. Hence, this shows much interest to use aqueous plant extract of *Vanda Testacea* as reducing agent for the preparation of metal sulphide nanoparticles by green bio-synthetic approach. Semiconducting metal sulphide nanoparticles that reduce the ability of the dye degradation were agglomerated without supporting materials. In order to avoid the agglomeration, the usage of the porous supporting materials is essential for metal sulphide photocatalyst. The use of porous supporting material protects metal sulphide from agglomeration and also gives enhanced effective adsorption and specific surface area to the photocatalyst. Therefore, the selection of porous materials like alumina, silica, ordered carbon such as carbon nanotube, graphene, mesoporous carbon, fullerene etc., and is important for photocatalyst. Triazine framework-based polymer-carbon nanotube composite has been chosen as porous supporting material for photocatalyst.

With this point of view, the present work is attempting to dope ZnS and ZnS-SnS nanoparticles on poly(cyanuric chloride-*co*-biphenyl)-carbon nanotube (Poly(CC-*co*-BP)-CNT) as supporting material by green biosynthetic approach for methylene blue dye degradation. Undoubtedly, this is the first work done on the synthesis of ZnS and ZnS-SnS nanoparticles doped Poly(CC-*co*-BP)-CNT as a supporting material by using aqueous plant extract of *Vanda Testacea.* The durability of prepared ZnS/ Poly(CC-*co*-BP)-CNT and ZnS-SnS/Poly(CC-*co*-BP)-CNT photocatalyst have been checked under same experimental condition towards methylene blue dye degradation. Additionally, the antimicrobial activity of the prepared ZnS/ Poly(CC-*co*-BP)-CNT and ZnS-SnS/Poly(CC-*co*-BP)-CNT photocatalyst tested against the microorganism namely *Bacillus thuringiensis, Escherichia coli*, *Pseudomonas aeruginosa and Staphylococcus aureus*.

2. EXPERIMENTAL METHODS

2.1. Materials

Vanda testacea, anhydrous Zinc (II) Chloride ($ZnCl_2$), Stannous (II) chloride dihydrate ($SnCl_2.2H_2O$), Sodium Sulphide (Na_2S), Potassium hydroxide (KOH), Methylene blue (MB) were purchased from SRL, India. Anhydrous $AlCl_3$ and multiwalled carbon nanotubes were purchased from Sigma Aldrich, India. Anhydrous $AlCl_3$ was purchased from Sigma Aldrich, India. Dichloromethane (DCM), cyanuric chloride (CC), biphenyl (BP), Peptone (Microbiology grade), Agar (Bacteriological grade) and Sodium Chloride (Laboratory reagent) were purchased from Merck, India.

2.2. Preparation of aqueous *Vanda Testacea* plant extract

Vanda testacea plant material was collected in Tirupati hills, Andhra Pradesh, India (April 2021) and is air dried for 15 days and is crushed into fine powder. This powder is named as *Vanda testacea* powder. The aqueous plant extract of *Vanda testacea* were prepared by microwave-Assisted method. For these 5 grams of *Vanda testacea* powder is dispersed in 100 ml of deionized water and kept in microwave oven for 5 mins at input power of 600 watts. After Cooling to room temperature, the aqueous plant extract is filtered and used as a reducing agent for the preparation photocatalyst.

2.3. Preparation of photocatalyst support poly(cyanuric chloride-*co*-biphenyl)-carbon nanotube (Poly(CC-*co*-BP)-CNT) composite

For the preparation photocatalyst support Poly(CC-*co*-BP)-CNT composite, 5 mg of carbon nanotube was dispersed in 25 ml of anhydrous dichloromethane. To the dispersed solution add 5 mg of cyanuric chloride and 15 mg of biphenyl. To the above reaction mixture 15 mg of anhydrous $AlCl_3$ catalyst was added to initiate the Friedel-Crafts reaction [56–58] and reaction mixture is refluxed at 65°C under inert atmosphere for 16 h. Then the reaction mixture was allowed to cool at 25°C. The obtained Poly(CC-*co*-BP)-CNT composite in reaction solution was filtered and its impurities were removed by washing several times with dichloromethane and distilled water and then the prepared Poly(CC-*co*-BP)-CNT composite dried at 110°C in an hot air oven for 24 h.

2.4. Preparation of Zinc Sulphide nanoparticles doped poly(cyanuric chloride-*co*- biphenyl)-carbon nanotube (ZnS/Poly(CC-*co*-BP)-CNT) by green bio-synthesis method

ZnS/Poly(CC-*co*-BP)-CNT photocatalyst was prepared by following procedure. At first, 20 mg of poly(cyanuric chloride-*co*-biphenyl)-carbon nanotube (Poly(CC-*co*-BP)-CNT) were dispersed in 20 ml of aqueous plant extract of *Vanda Testacea* in a clean 100 ml round bottom flask. To the dispersed mixture 0.4 M of $ZnCl_2$ metal precursor solution is added and stirred for 1 hour. After that 0.4 M freshly prepared Na_2S solution were added slowly to the reaction mixture and the obtained suspension is continuously stirred for another 4 hours. The obtained ZnS/Poly(CC-*co*-BP)-CNT was centrifuged, washed and dried at 110°C for 24 hours. For Poly(CC-*co*-BP)-CNT optimization, the Poly(CC-*co*-BP)-CNT is taken in different weight percentage of 0.5%, 1.0% and 1.5% with respect to weight of $ZnCl_2$ metal precursor.

2.5. Preparation of Zinc Sulphide-Sin Sulphide nanoparticles doped poly(cyanuric chloride-*co*-biphenyl)-carbon nanotube (ZnS-SnS/Poly(CC-*co*-BP)-CNT) by green bio-synthesis method

ZnS-SnS/Poly(CC-*co*-BP)-CNT were prepared by taking 1% wt of Poly(CC-*co*-BP)-CNT composite by using 0.2 M $ZnCl_2$ and 0.2 M $SnCl_2.2H_2O$ and 0.8 M Na_2S as precursor solution. 1 wt % of Poly(CC-*co*-BP)-CNT support was dispersed in 20 ml of aqueous plant extract of *Vanda Testacea* in a clean 100 ml round bottom flask. To the above suspension add 0.2 M $ZnCl_2$ and 0.2 M $SnCl_2.2H_2O$ precursor solution and stirred for 1 hour. To this reaction mixture add 0.4 M of freshly prepared sodium sulphide solution (Na_2S) and stir the mixture for 4 hours. The obtained ZnS^{1}-SnS^{1}/Poly(CC-*co*-BP)-CNT photocatalyst were centrifuged, washed and dried at 110°C for 24 hours. For the optimization of Sn in ZnS-SnS/Poly(CC-*co*-BP)-CNT photocatalyst, the ZnS^{1}-$SnS^{0.25}$/Poly(CC-*co*-BP)-CNT, ZnS^{1}-$SnS^{0.5}$/ Poly(CC-*co*-BP)-CNT and ZnS^{1}-$SnS^{0.75}$/ Poly(CC-*co*-BP)-CNT photocatalyst were prepared by similar experimental procedure.

2.6. Characterization techniques

The surface analysis of the prepared poly(cyanuric chloride-co-biphenyl)-carbon nanotube (Poly(CC-*co*-BP)-CNT), poly(cyanuric chloride-co- biphenyl) (Poly(CC-*co*-BP) and carbon nanotube (CNT) were characterized by Fourier Transform Infrared (Cary 630, Agilent technologies, USA) Spectroscopy, X-ray diffraction (Rigaku Mixfix 600, Rigaku corporation, Japan) patterns were analysed at 25°C temperature. The active surface area of the prepared material was measured by BET analysis (Quanta chrome Instruments, Autos orb IQ series). The surface of the prepared materials was examined by Scanning Electron Microscope (JEOL, JEM-2100 Plus, Japan) and Energy Dispersive Spectroscopy (EDAX-EDS-SDD. EDAX Inc., USA). Finally, the average particles size of the prepared ZnS and ZnS-SnS were analysed by High Resolution Transmission Electron Microscope (HR-TEM, JEOL, USA) with an accelerating voltage of 120 kV.

2.7. Measurement of Phenol, Protein, Flavonoid, Reducing sugar, and Anthocyanin constituents of *vanda Testacea plant* extract

Prior to the preparation of ZnS and ZnS-SnS doped Poly(CC-*co*-BP)-CNT photocatalyst it is essential to measure the constituents present in the *vanda Testacea plant* extract [59–62].

2.8. Photo degradation experiments

The dye degradation was carried out by photocatalytic irradiation method using photoreactor (Heber scientific multilamp, India). The photoreactor chamber consists of mercury vapour lamps (8W) set in parallel and with emitting wavelength of 365 nm and it have the reflector which is made of high polished aluminium with inbuilt cooling fan. Further, the photoreactor have the in-build magnetic stirrer and with

reaction glass tube of capacity of 50 mL. The 10 mg photocatalyst were dispersed 50 mL of 12 PPM dye solution and it was stirred for 30 mins in dark condition before starting photocatalytic irradiation which allows the absorption of dye on the photocatalyst surface. During dye degradation by photocatalyst, 3–5 mL of the degrading samples were collected at uniform time interval. Then, it was centrifuged to remove the photocatalyst present in the collected solution. The absorbance is measured for collected dye solution at different time interval using Ultra Violet-Visible spectrophotometer.

3. RESULTS AND DISCUSSION

3.1. Phenol, Protein, Flavonoid, Reducing sugar, and Anthocyanin constituents of *vanda Testacea plant* extract

It is essential to measure the total phenol, flavonoid, reducing sugar, anthocyanin and total protein present in *vanda Testacea plant* extract using precise methods. Table 1 displays the values of compounds. From the values it was observed that the *Vanda Testacea* plant extract were abundant in total phenolic compounds (34.67 ± 4.45 mg g^{-1} FW), flavonoids (23.84 ± 2.48 mg g^{-1} FW), reducing sugar (2.26 ± 0.49 mg g^{-1} FW), anthocyanin (5.64 ± 0.04 µg g^{-1} FW) and total protein (2.48 ± 0.64 mg g^{-1} FW). From the results it was proposed that various compound present in *vanda Testacea plant* extract may play a role in the formation of nanoparticles on Poly(CC-*co*-BP)-CNT surface.

Table 1
Protein, reducing sugar, anthocyanin, phenolic and flavonoid content in plant extract of fenugreek

Total Phenolic (mg g^{-1} FW)	Flavonoid (mg g^{-1} FW)	Reducing Sugar (mg g^{-1} FW)	Anthocyanin (µg g^{-1} FW)	Total Protein (mg g^{-1} FW)
34.67 ± 4.45	23.84 ± 2.48	2.26 ± 0.49	5.64 ± 0.04	2.48 ± 0.64

3.2. Fourier Transform InfraRed analysis

FT-IR spectra of poly(cyanuric chloride-*co*-biphenyl) composite (Poly(CC-*co*-BP) and poly(cyanuric chloride-*co*-biphenyl)-carbon nanotube composite (Poly(CC-*co*-BP)-CNT) were shown in Fig. 1**(a-b)**. In Fig. 1**(a)**, the characteristic triazine peak observed at 1364 cm^{-1} and 1507 cm^{-1} of cyanuric chloride monomers and the phenyl moiety characteristic peak observed at 1622 cm^{-1} and 774 cm^{-1} of biphenyl monomer. The disappearance of characteristic C-Cl peaks at 850 cm^{-1} [63–66], which confirms cyanuric chloride and biphenyl monomers involve in the formation of Poly(CC-*co*-BP) composite.

Further, in the Fig. 1**(b)** of Poly(CC-*co*-BP)-CNT composite also exhibits comparable characteristic peaks observed for Poly(CC-*co*-BP) composite. These confirms the presence of Poly(CC-*co*-BP) on the surface of CNT material through non-covalent interaction.

3.3. X-Ray diffraction analysis

The XRD patterns of ZnS/Poly(CC-*co*-BP)-CNT and ZnS-SnS/Poly(CC-*co*-BP)-CNT were shown in Fig. 2. In Fig. 2(a) for ZnS in ZnS/Poly(CC-*co*-BP)-CNT exhibits four peaks at 28.03˚, 46.45˚, 55.20˚ and 57.36˚ and it represents the formation of ZnS nanoparticles with cubic structure (JCPDS no. 05 0566) [67, 68] Fig. 2(b) shows the XRD pattern of ZnS-SnS/Poly(CC-*co*-BP)-CNT photocatalyst. In Fig. 2(b) the ZnS exhibits four peaks which is comparable to ZnS peaks in Fig. 2(a). Further, SnS exhibits three more peaks at 32.40˚, 35.15˚ and 38.09˚ these represents the SnS is orthorhombic structure (JCPDS no. 39–0354) [69–71]. From the XRD result it was concluded that ZnS and ZnS-SnS doped on the surface of Poly(CC-*co*-BP)-CNT composite.

3.4. Ultra Violet-Diffuse reflectance spectra analysis (UV-DRS)

The optical property of unsupported ZnS and ZnS/Poly(CC-*co*-BP)-CNT photocatalyst were analysed using Ultra Violet-Diffuse Reflectance Spectra. Figure 3 shows Ultra Violet-Diffuse Reflectance Spectra of unsupported ZnS and ZnS/Poly(CC-*co*-BP)-CNT photocatalyst. The wavelength of the ZnS/Poly(CC-*co*-BP)-CNT photocatalyst is found to greater that of the unsupported ZnS photocatalyst. Here, ZnS/Poly(CC-*co*-BP)-CNT photocatalyst shows red shifts when compared with unsupported ZnS photocatalyst. The band gap energy values were calculated for unsupported ZnS and ZnS/Poly(CC-*co*-BP)-CNT photocatalyst and it values is 3.72 eV and 3.28 eV [72, 73]. The decreased band gap energy of ZnS/Poly(CC-*co*-BP)-CNT photocatalyst is because of the synergistic chemical interaction between ZnS and the support Poly(CC-*co*-BP)-CNT composite. This decreased band gap energy of ZnS/Poly(CC-*co*-BP)-CNT photocatalyst shows a broader absorption in the ultra violet region than the unsupported ZnS photocatalyst, so it can generate more electron-hole pairs in UV irradiation. Generally, the decreased band gap energy value of the photocatalyst improve the photocatalytic activity of the catalyst [74–76] The UV-DRS studies is used as supplementary evidence for the enhancement photocatalytic activity of dye degradation for wastewater treatment applications. So, ZnS/Poly(CC-*co*-BP)-CNT photocatalyst shows enhanced photocatalytic activity than that of the unsupported ZnS photocatalyst towards methylene blue dye degradation.

3.5. Photoluminescence (PL) Studies

Photoluminescence studies were carried out for unsupported ZnS and different weight percentage of Poly(CC-*co*-BP)-CNT in ZnS/Poly(CC-*co*-BP)-CNT (ZnS/0.25% Poly(CC-*co*-BP)-CNT, ZnS/0.5% Poly(CC-*co*-BP)-CNT, ZnS/0.75% Poly(CC-*co*-BP)-CNT and ZnS/1% Poly(CC-*co*-BP)-CNT) photocatalyst at room temperature. Figure 4 shows the photoluminescence spectra of unsupported ZnS and weight percentage of ZnS/Poly(CC-*co*-BP)-CNT photocatalysts. The emission band for unsupported ZnS and different weight percentage of Poly(CC-*co*-BP)-CNT in ZnS/Poly(CC-*co*-BP)-CNT photocatalysts were observed at 410 and 450 nm. The weak emission peak at 410 nm was attributed to the surface defects and vacancies of the ZnS nanoparticles [77].

From the PL spectra of unsupported ZnS and different weight percentage of Poly(CC-*co*-BP)-CNT composite in ZnS/Poly(CC-*co*-BP)-CNT photocatalyst, it has been detected that the intensity of the emission peak (photoluminescence) decreases with increase weight of Poly(CC-*co*-BP)-CNT in ZnS/Poly(CC-*co*-BP)-CNT photocatalyst. This indicates that PL quenching occurs because of the chemical interaction between the ZnS and Poly(CC-*co*-BP)-CNT in ZnS/Poly(CC-*co*-BP)-CNT photocatalyst. Subsequently, the addition of Poly(CC-*co*-BP)-CNT to ZnS reduces the recombination of electron-hole pairs which reduces the defects and vacancies in ZnS photocatalyst. So, ZnS/Poly(CC-*co*-BP)-CNT can be used as an active catalyst towards dye degradation.

3.6. BET analysis

Photocatalysis process is surface-based process which requires more active sites. Heterogeneous photocatalyst well recognized for its high surface area is important to produce more active sites that can increase the shed light on the surface of the photocatalyst. Thus, improves the photocatalytic activity of the photocatalyst. The photocatalytic activity of the photocatalyst was determined by their active surface area. It has been broadly known that the prepared photocatalyst possessed with porous nature this gives hight active surface area. The porous nature of the photocatalyst will allow the transportation of reactants and products through interior space is due to the interconnected porous network and its cares the gathering of excited light because of high surface area and many scatterings occurs within the porous framework [78, 79]. The active surface area of the prepared Poly(CC-*co*-BP)-CNT composite, Zinc sulphide (ZnS) and different weight percentage of Poly(CC-*co*-BP)-CNT in ZnS/Poly(CC-*co*-BP)-CNT were measured by Nitrogen adsorption-desorption isotherms (Fig. 5).

The BET surface is Poly(CC-*co*-BP)-CNT composite, unsupported ZnS, ZnS/0.25% Poly(CC-*co*-BP)-CNT, ZnS/0.5% Poly(CC-*co*-BP)-CNT, ZnS/1% Poly(CC-*co*-BP)-CNT and ZnS/1.25% Poly(CC-*co*-BP)-CNT photocatalysts are 6.4, 65.1, 77.4, 95.8, 155.6 and 131.5 m^2/g, respectively. Hence, ZnS/1% Poly(CC-*co*-BP)-CNT photocatalyst owns a high surface area than other photocatalysts. Further, the surface area of the photocatalyst were increased with increase in the weight percentage of Poly(CC-*co*-BP)-CNT in ZnS/Poly(CC-*co*-BP)-CNT photocatalyst. In the present study, 1% weight of Poly(CC-*co*-BP)-CNT in ZnS/Poly(CC-*co*-BP)-CNT photocatalyst exhibits high specific surface are when compared with other photocatalyst. So, ZnS/1% Poly(CC-*co*-BP)-CNT photocatalyst have a greater number of active adsorptions cites for dye adsorption and also harvest more light source. Hence, the high specific surface is essential to achieve highly active photocatalyst.

3.7. Scanning Electron Microscope and Energy Dispersive X-Ray analysis

Figure 6 shows the EDAX spectra of ZnS/Poly(CC-*co*-BP)-CNT photocatalyst. The EDAX spectra confirms the presence of Zn and S elements in ZnS/Poly(CC-*co*-BP)-CNT photocatalyst. Figure 7 shows the EDAX spectra of ZnS-SnS/Poly(CC-*co*-BP)-CNT photocatalyst. Further, the EDAX spectra confirms the presence of Zn, Sn and S elements in ZnS-SnS/Poly(CC-*co*-BP)-CNT photocatalyst.

3.8. High Resolution Transmission Electron Microscope analysis

The morphology and particle size of ZnS and ZnS-SnS doped ZnS-SnS/Poly(CC-*co*-BP)-CNT photocatalyst were examined by Transmission electron microscope image. From the Fig. 8 it was clearly visualized the ZnS and ZnS-SnS nanoparticles were uniformly dispersed on the surface of Poly(CC-*co*-BP)-CNT supporting materials without aggregation of nanoparticles. The particles size of ZnS and ZnS-SnS nanoparticle is approximately 3–4 nm.

3.9. XPS Analysis

X-ray photoelectron spectroscopy (XPS) measurement have been carried out for ZnS-SnS/Poly(CC-*co*-BP)-CNT photocatalyst (Fig. 9). The full scan XPS spectrum have been shown in Fig. 9(a) for ZnS-SnS/Poly(CC-*co*-BP)-CNT which also the confirms the presence of Zn, Sn and S present in ZnS-SnS/Poly(CC-*co*-BP)-CNT photocatalyst. Figure 9 (b, c and d) shows the XPS spectra for Zn(2p), Sn (3d) and S(2p), respectively. The observed binding energies values are concords with the literature data [80–83]. Thus, exhibits the interaction among the Zn, Sn and S in the ZnS-SnS/Poly(CC-*co*-BP)-CNT photocatalyst.

3.10. Photodegradation of methylene blue dye

The methylene blue dye degradation has been carried out for unsupported ZnS and ZnS/ Poly(CC-*co*-BP)-CNT photocatalyst under optimized condition of 12 ppm of methylene blue solution and 50 mg of photocatalysts under natural sun light and three different UV irradiation sources [UV-1 (350 nm), UV-2 (310 nm) and UV-3 (254 nm)]. The methylene blue dye degradation evolution has been supervised using UV-visible spectroscopy analysis at various time intervals in the presence of unsupported ZnS and ZnS/Poly(CC-*co*-BP)-CNT photocatalyst, were shown in Fig. 10 and Fig. 11.

Figure 10 **(a & b)** shows the measurement of UV-Visible spectra of methylene blue dye degradation at various time intervals under natural sun light and UV3 irradiation. From the Fig. 10 (a & b), it has been observed that the methylene blue solution exhibits an absorption peak at 664 nm. The intensity of the absorption peak decreases with increase in irradiation time. The complete methylene blue dye degradation occurs within 210 mins and 120 mins for unsupported ZnS photocatalyst under natural sun light and UV3 irradiation.

Figure 11 **(a & b)** shows the measurement of UV-Visible spectra of methylene blue dye degradation at various time intervals under natural sun light and UV3 irradiation. From the Fig. 11 (a & b), it has been observed that the methylene blue solution exhibits an absorption peak at 664 nm. The intensity of the absorption peak decreases with increase in irradiation time. The complete methylene blue dye degradation occurs within 180 mins and 60 mins for ZnS/1% Poly(CC-*co*-BP)-CNT photocatalyst under natural sun light and UV3 irradiation.

From the Fig. 10(b) and 11(b), it was concluded that methylene blue dye degradation takes effectively in the presence of the ZnS/1%Poly(CC-*co*-BP)-CNT photocatalyst under UV3 irradiation (wavelength = 254 nm). In addition to that supported ZnS/1%Poly(CC-*co*-BP)-CNT photocatalyst is also found to be effective than unsupported ZnS photocatalyst towards methylene blue dye degradation in other two UV irradiation sources. Hence, Poly(CC-*co*-BP)-CNT is a good supporting material for ZnS nanoparticles for photocatalytic activities. This enhanced photocatalytic activity of ZnS/1%Poly(CC-*co*-BP)-CNT photocatalyst may be due to the synergistic chemical interaction between the Poly(CC-*co*-BP)-CNT and ZnS nanoparticles present in the ZnS/1%Poly(CC-*co*-BP)-CNT photocatalyst and the exposed UV3 irradiation light energy is well synchronized with the band gap values of ZnS/1%Poly(CC-*co*-BP)-CNT photocatalyst. Therefore, maximum electron-hole pair density was gained, which leads to the rapid photocatalytic reaction [84].

Further, the time required for methylene blue dye degradation in different light sources was shown in the Table 2. The percentage of methylene blue dye degradation was calculated by the following Eq. (1)

$$D\,(\%) = \frac{C_0 - C_t}{C_0} \times 100 - - - (1)$$

where, D dye degradation rate, C_0 is the absorption of dye at 0 min and C_t is the absorption of dye at time in minutes for the irradiation.

Table 2
Time required for different light source to complete methylene blue dye degradation in the presence of unsupported ZnS and ZnS/1% Poly(CC-*co*-BP)-CNT photocatalyst.

Photocatalyst	MB solution	Light source	Time (mins)	% of degradation
Unsupported ZnS	12 ppm	Sun light	210	95
		UV1	180	95
		UV 2	150	95
		UV3	120	95
ZnS/1% Poly(CC-*co*-BP)-CNT	12 ppm	Sun light	180	95
		UV1	120	94
		UV 2	90	94
		UV3	60	100

The above interesting result makes the author to extend the work to furthermore. So, the addition of SnS (different weight % 0.25, 0.50, 0.75 and 1.00) to ZnS/Poly(CC-co-BP)-CNT photocatalyst. The photocatalytic activity of the prepared ZnS^{1}-$SnS^{0.25}$/Poly(CC-co-BP)-CNT, ZnS^{1}-$SnS^{0.50}$/Poly(CC-co-BP)-

CNT, ZnS^{1}-$SnS^{0.75}$/Poly(CC-co-BP)-CNT and ZnS^{1}-SnS^{1}/Poly(CC-co-BP)-CNT photocatalyst (50 mg) is tested towards methylene blue dye degradation (12 PPM) under and UV3 irradiation (Wavelength – 254 nm) sources. Table 3 shows percentage of methylene blue dye (12 PPM) degradation in 30 minutes for the various ratio of ZnS-SnS/Poly(CC-co-BP)-CNT photocatalyst (50 mg) under UV3 irradiation (Wavelength – 254 nm) source.

Table 3
Percentage of methylene blue dye (12 PPM) degradation in 30 minutes for the various ratio of ZnS-SnS/Poly(CC-co-BP)-CNT photocatalyst (50 mg) under UV3 irradiation (Wavelength – 254 nm) source

Photocatalyst	MB solution	Light source	Time (mins)	% of degradation
ZnS^{1}-$SnS^{0.25}$/Poly(CC-co-BP)-CNT	12 ppm	UV3 irradiation	30	68
ZnS^{1}-$SnS^{0.50}$/Poly(CC-co-BP)-CNT				74
ZnS^{1}-$SnS^{0.75}$/Poly(CC-co-BP)-CNT				86
ZnS^{1}-SnS^{1}/Poly(CC-co-BP)-CNT				100

From the above result, it was it was observed the 100% methylene blue dye degradation take place in 30 mins for $ZnS^{1}SnS^{1}$/1% Poly(CC-*co*-BP)-CNT (50 mg) photocatalyst under UV3 irradiation. But the other ratio of $ZnS^{1}SnS^{0.25}$/1% Poly(CC-*co*-BP)-CNT, $ZnS^{1}SnS^{0.5}$/1% Poly(CC-*co*-BP)-CNT and $ZnS^{1}SnS^{0.75}$/1% Poly(CC-*co*-BP)-CNT photocatalyst degrades 68%, 74% and 86% under similar experimental condition. The photocatalytic activity $ZnS^{1}SnS^{1}$/1%Poly(CC-*co*-BP)-CNT photocatalyst is found to greater that than other photocatalyst is may because of synergic effect or interaction between ZnS and SnS in $ZnS^{1}SnS^{1}$/1% Poly(CC-*co*-BP)-CNT photocatalyst that decrease the electron-hole pair recombination effect and it improve the life time of the photogenerated electron-hole pairs. Therefore, maximum electron-hole pair density was gained, which leads to the rapid photocatalytic reaction [84].

3.11. Kinetics Studies for methylene blue dye degradation using $ZnS^{1}SnS^{1}$/1%Poly(CC-co-BP)-CNT photocatalyst

The MB dye degradation was investigated in the presence of $ZnS^{1}SnS^{1}$/1%Poly(CC-*co*-BP)-CNT photocatalyst which follows the pseudo-first order kinetics. The performance of the $ZnS^{1}SnS^{1}$/1%Poly(CC-*co*-BP)-CNT photocatalyst will affect by the weight of the photocatalyst and concentration of the methylene blue dye solution. So, kinetics studies were carried out by varying the weight of the photocatalyst and concentration of the methylene blue dye solution.

3.11.1. Effect of methylene blue dye concentration

The kinetic studies of the concentration of methylene blue dye degradation were investigated by varying the concentration of the MB dye from 4, 8, 12 and 16 ppm. Figure 13 shows the effect of MB dye on

ZnS^1SnS^1/1%Poly(CC-*co*-BP)-CNT photocatalyst at 10 mins of irradiation time. The concentration of MB dye increases, which increases the greater number of MB dye molecules adsorbing on the surface of ZnS^1SnS^1/1%Poly(CC-*co*-BP)-CNT photocatalyst. Hence, it is likely to improve the photocatalytic activity towards MB dye degradation.

At the higher MB dye concentration, the penetration of the photons from light source to the photocatalyst surface was reduced these exhibits the least formation of hydroxy radicals for the MB dye degradation process [85]. As a result, the rate of MB dye degradation decreases with an increase in the concentration of MB dye.

3.11.2. Effect of photocatalyst weight

The effect of ZnS^1SnS^1/1%Poly(CC-*co*-BP)-CNT photocatalyst weight was investigated by varying the catalyst weight of 10, 30, 50, 70 and 100 mg in 12 ppm of MB dye solution after 10 minutes. Figure 14 shows plots of different weight of ZnS^1SnS^1/1%Poly(CC-*co*-BP)-CNT photocatalyst weight versus rate of MB dye degradation. The MB dye degradation on varying the photocatalyst weight also follows the pseudo-first order reaction. From the Fig. 14 it was noticed, that the increase in the weight of the photocatalyst (increase the illumination area) leads to increase in the surface area of the photocatalyst. So, adsorption of the MB dye molecules also increases on the photocatalyst surface [85].

3.12. Mechanism of photodegradation of MB over ZnS^1SnS^1/1%Poly(CC-co-BP)-CNT nanocomposite

Figure 15 shows the proposed degradation mechanism of methylene blue dye using ZnS^1SnS^1/1%Poly(CC-*co*-BP)-CNT photocatalyst. In a degradation reaction, breaking and formation of bond takes place. According to bond dissociation energy (BDE) theory, if the BDE is less breaking of the old bond and formation of new bond takes place easily. Degradation mechanism of methylene blue is analyzed based on intermediate and products. During the dissolution of methylene molecule Cl^- is first ionized and exists in the detached state. N-CH_3 has low BDE during the bombardment of the radical species, N-CH_3 bond is easily broken and -CH_3 is oxidized to HCHO and HCOOH. C-S and C-N are the next most active parts in the methylene blue molecule during bombardment of •OH and O_3, the two bonds are easily broken. In Dielectric barrier discharge (DBD) process [86], an abundance of radical species in the methylene blue solution is generated. These oxidize organic molecular structures until they are finally transformed into inorganic ions like NO_3^-,SO_4^{2-}, C, CO_2 and H_2O [87].

3.13. Reusability of the ZnS^1SnS^1/1%Poly(CC-co-BP)-CNT photocatalyst

It is very important to check the durability of the ZnS^1SnS^1/1%Poly(CC-*co*-BP)-CNT photocatalyst MB dye degradation under UV3 irradiation. So, the reusability and stability of ZnS^1SnS^1/1%Poly(CC-*co*-BP)-CNT photocatalyst were determined by undergoing the MB dye degradation on same catalyst for three times.

It was noticed, in Fig. 16 that there is no remarkable change in the photocatalytic activity of $ZnS^{1}SnS^{1}$/1%Poly(CC-*co*-BP)-CNT after repeating the MB dye degradation for three times.

4. CONCLUSION

A green biosynthetic approach is used to dope ZnS nanoparticles on the surface Poly(cyanuric chloride-*co*-biphenyl)-CNT composite (Poly(CC-*co*-BP)-CNT) (different weight percentage 0.25, 0.5, 1 and 1.25%) using *Vanda testacea* plant extract as reducing agent. The prepared ZnS/Poly(CC-*co*-BP)-CNT were characterised by UV-Visible DRS, PL, EDX, TEM and BET techniques. The BET analysis concludes that 1% Poly(CC-*co*-BP)-CNT supported ZnS has a higher surface area than other ZnS/0.25% Poly(CC-*co*-BP)-CNT, ZnS/0.5% Poly(CC-*co*-BP)-CNT and ZnS/1.25% Poly(CC-*co*-BP)-CNT and unsupported ZnS photocatalyst. The photocatalytic activity of supported ZnS/1% Poly(CC-*co*-BP)-CNT and unsupported ZnS photocatalyst were tested towards methylene blue dye degradation under visible light and various wavelength of UV light (UV1-350 nm, UV2- 310 nm and UV3-254 nm). From the methylene blue dye degradation result it was concluded that ZnS/1% Poly(CC-*co*-BP)-CNT (50 mg) photocatalyst is an efficient photocatalyst than other and unsupported ZnS photocatalyst towards methylene blue dye (12 PPM) degradation under UV3 irradiation. This may due to the synergistic chemical interaction between the Poly(CC-*co*-BP)-CNT and ZnS nanoparticles present in the ZnS/1%Poly(CC-*co*-BP)-CNT photocatalyst. Further, the work is extended to next step different weigh ratio of SnS (weight percentage of 0.25%, 0.5%, 0.75% and 1%) is added with ZnS/1%Poly(CC-*co*-BP)-CNT photocatalyst. The photocatalytic activity of the prepared photocatalyst towards methylene dye degradation. From the result, it was found that $ZnS^{1}SnS^{1}$/1%Poly(CC-*co*-BP)-CNT (50 mg) photocatalyst involve 100% of methylene blue dye (12 PPM) degradation in 30 minutes under UV3 light sources than other photocatalyst and this may because of synergic effect or interaction between ZnS and SnS in $ZnS^{1}SnS^{1}$/1% Poly(CC-*co*-BP)-CNT photocatalyst which decrease the electron-hole pair recombination effect and it improve the life time of the photogenerated electron-hole pairs. Therefore, maximum electron-hole pair density was gained, which leads to the rapid photocatalytic reaction. The stability and efficiency of the $ZnS^{1}SnS^{1}$/1% Poly(CC-*co*-BP)-CNT photocatalyst were tested under similar experimental condition and the results conclude that the prepared $ZnS^{1}SnS^{1}$/1% Poly(CC-*co*-BP)-CNT is a reusable photocatalyst. Because of durability the prepared $ZnS^{1}SnS^{1}$/1% Poly(CC-*co*-BP)-CNT can be recommended for dye degradation in industries. Hence, the prepared $ZnS^{1}SnS^{1}$/1% Poly(CC-*co*-BP)-CNT photocatalyst is a promising material for the removal of MB dye.

Declarations

ACKNOWLEDGMENT

This work was supported by The Honourable Chairman, Vignan's Group of Education Institutions, Andhra Pradesh. Further the authors the extended the heartfelt thanks to The Chairman, Principal and Head of the Department Vignan's Nirula Institute of Technology and Science, Guntur, Andhra Pradesh, India.

Ethical Approval: Not applicable

Competing interests: Not applicable

Authors' contributions:

S. RatnaKumari: Writing – review & editing.

Dr.D. Prasanna: Conceptualization, Methodology, Investigation.

Dr.V.Anuradha & Dr.T.Raja Rajeswari: Resources, Supervision.

Funding: No Financial support

Availability of data and materials: Original data have been included in the manuscript.

References

1. N. Rajesh Jesudoss Hynes, J. Senthil Kumar, Hesam Kamya, J. Angela Jennifa Sujana, Omar Ali Al-Khashman, Yasemin Kuslu, Antoaneta Ene, B.Suresh Kumar, J. Clean. Prod., 2020, 272, 122636.
2. Houda Ben Slama, Ali Chenari Bouket, Zeinab Pourhassan, Faizah N. Alenezi, Allaoua Silini, Hafsa Cherif-Silini, Tomasz Oszako, Lenka Luptakova, Patrycja Golinska, Lassaad Belbahri, Appl. Sci. 2021, 11, 6255.
3. Bruno Lellis, Cíntia Zani Fávaro-Polonio, João Alencar Pamphile, Julio Cesar Polonio,, Biotechnol. Res. Innovation., 2019, 3, 275–290.
4. Mohamed Berradi, Rachid Hsissou, Mohammed Khudhair, Mohammed Assouag, Omar Cherkaoui, Abderrahim El Bachiri, Ahmed El Harfi, Heliyon, 2019, 5, 02711.
5. Ben van den Akker, Mike Holmes, Peter Pearce, Nancy J. Cromar, Howard J. Fallowfield, Water Res., 2011, 45, 3489–3498.
6. S. Rangabhashiyam, Pollyanna V. dos Santos Lins, Leonardo M.T. de Magalhães Oliveira, Pamela Sepulveda, Joshua O. Ighalo, Anushka Upamali Rajapaksha, Lucas Meili, Environ. Pollut., 2022, 293, 118581.
7. Kwang-Ho Choo, Dae-Ic Chang, Kyong-Won Park, Moon-Hyeon Kim, Use of an integrated photocatalysis/hollow fiber microfiltration system for the removal of trichloroethylene in water, J. Hazard. Mater., 2008, 152, 183–190.
8. Changsheng Peng, Linheng Chen, Xiange Wu, Xixi Wei, Aafia Tehrim, Min Dai, Simin Xu, J. Environ. Chem. Eng., 2021, 9, 105690.
9. Tamara Kawther Hussein, Nidaa Adil Jasim, Mater. Today: Proc., 2021, 42, 1946–1950.
10. Jiade Wang, Tian Zhang, Yu Mei, Bingjun Pan, Chemosphere, 2018, 201, 621–626.
11. Xian Liu, Shihao Shen, Chengxiang Xu, Xiaoya Li, Lei Zhu, Xun Wang, Mater. Today Chem., 2022, 23, 100667.

12. Seong Youl Lee, Hoang Tung Do, Joon Heon Kim, Appl. Surf. Sci., 2022, 573, 151383.
13. Junwei Hou, Hedong Yang, Boyao He, Jingui Ma, Yuan Lu, Qingyao Wang, Fuel, 2022, 310, 122364.
14. Sachin S. Kushare, Vivek D. Bobade, Dipak R. Tope, Ashok V. Borhade, J. Indian Chem. Soc, 2021, 98, 100239.
15. S. Sugashini, T. Gomathi, R. Aruna Devi, P.N. Sudha, K. Rambabu, Fawzi Banat, Environ. Res., 2022, 204, 112047.
16. Meroua Safa Mechouche, Fateh Merouane, Chemes El Houda Messaad, Nasrin Golzadeh, Yasser Vasseghian, Mohammed Berkani, Environ. Res., 2021, 204, 112360.
17. Roselin Ranjitha Mathiarasu, Ayyar Manikandan, Kurinjinathan Panneerselvam, Mary George, K. Kanmani Raja, M.A. Almessiere, Y. Slimani, A. Baykal, Abdullah M. Asiri, Tahseen Kamal, Anish Khan, J. Mater. Res. Technol., 2021, 15, 5936–5947.
18. Qiao Yang, Jingcheng Hao, Colloids Surf., A, 2022, 633, 127848.
19. Yingbo Song, Dedong Sun, Xinyu Jiang, Huanran Ma, Chun Ma, Jun Hao, Xinxin Zhang, J. Environ. Chem. Eng., 2021, 9, 106889.
20. S. Munyai, N.C. Hintsho-Mbita, Curr. Res. Green Sustainable Chem., 2021, 4, 100163.
21. Natarajan Prakash, Ramachandran Balaji, Saravanan Govindaraju, Alexander Pinky Steffi, Nagendran Santhanalakshmi, Kumar Mohanraj, Ethiraj Selvarajan, Narendhar Chandrasekar, Melvin S. Samuel, Environ. Res., 2021, 204, 112383.
22. C. Anushree, D. Nanda Gopala Krishna, John Philip, J. Mol. Liq., 2021, 337, 116429.
23. Farheen Khurshid, M. Jeyavelan, S. Nagarajan, Synth. Met., 2021, 278, 116832.
24. Summal Zoha, Muneeb Ahmad, Syed Jazib Abbas Zaidi, Muhammad Naeem Ashiq, Waheed Ahmad, Tae Joo Park, Muhammad Abdul Basit, J. Photochem. Photobiol., A, 2020, 394, 112472.
25. María José Cortés Burgos, Simón Roa, Bayron Cerda, Paulraj Manidurai, Solid State Commun., 2021, 340, 114523.
26. Varun A. Chhabra, Rajnish Kaur, Manrajvir S. Walia, Ki-Hyun Kim, Akash Deep, Environ. Res., 2020, 186, 109615.
27. Sohel Das, Prathap Somu, Subhankar Paul, J. Mol. Liq., 2021, 340, 117055.
28. D.V. Sridevi, V. Ramesh, E. Sundaravadivel, Mater. Today: Proc., 2021, 42, 1244–1250.
29. Gururaj M. Neelgund, Aderemi Oki, Appl. Surf. Sci., 2021, 566, 150648.
30. S. Irudhaya Raj, Adhish Jaiswal, J. Photochem. Photobiol., A, 2021, 410, 113158.
31. Pazhanivel Devendran, Duraisamy Selvakumar, Govindarajan Ramadoss, Ramachandran Sivaramakrishnan, Thangavel Alagesan, Ramasamy Jayavel, Kannaiyan Pandian, Chemosphere, 2022, 287, 132091.
32. Surbhi Sharma, Dheeraj Kumar, Neeraj Khare, Polymer, 2021, 231, 124117.
33. Run-Sheng Lin, Taewan Kim, Xiao-Yong Wang, Wei Du, J. Cleaner Prod., 2022, 330, 129947.

34. Prateek Sharma, Mrityunjay Kumar Singh, Mohan Singh Mehata, Journal of Molecular Structure, 2022, 1249, 131651.
35. J. Srivind, V.S. Nagarethinam, M. Suganya, S. Balamurugan, D. Prabha, A.R. Balu, Mater. Sci. Eng., B, 2020, 255, 114530.
36. Love Dashairya, Manisha Sharma, Soumen Basu, Partha Saha, J. Alloys Compd., 2019, 774, 625–636.
37. Sabri Ouni, Naim Bel Haj Mohamed, Mohamed Bouzidi, Adrian Bonilla-Petriciolet, Mohamed Haouari, J. Environ. Chem. Eng., 2021, 9, 105915.
38. Rupy Dhir, Chem. Phys. Impac., 2021, 3, 100027.
39. Medha Bhushan, Ranjana Jha, Rekha Bhardwaj, J. Phys. Chem. Solids, 2019, 135, 109021.
40. Yonghui Lee, Dong Sik Kim, Sang Woo Jin, Hanchan Lee, Yu Ra Jeong, Ilhwan You, Goangseup Zi, Jeong Sook Ha, Chem. Eng. J., 2022, 427, 130858.
41. Alireza Goudarzi, Sanaz Mehdizadeh Langroodi, Mahdi Arefkhani, Narges Samadani Langeroodi, Mater. Chem. Phys., 2022, 275, 125103.
42. Fujun Zhang, Zheng Xu, Ling Liu, Lijian Meng, J. Rare Earths, 2006, 24, 298–301.
43. Priyanka Uddandarao, Raj Mohan Balakrishnan, Spectrochim. Acta, Part A, 2017, 175, 200–207.
44. G. Chabrier, J.P. Dufour, G. Niquet, P. Vernier, Thin Solid Films, 1985, 125, 123–127.
45. Xing Liu, Jiaqi Zhu, Jiecai Han, Int. J. Heat Mass Transfer, 2018, 124, 124–130.
46. Cheng-Shane Chu, Chih-Jen Su, Sensors and Actuators B: Chemical, 2018, 255, 1079–1086.
47. Sung I Ahn, Seong Eui Lee, Won Hee Lee, Shang Hyeun Park, Kyung Cheol Choi, Chem. Phys. Lett., 2010, 493, 113–117.
48. Arun Kumar, Manjeet Kumar, Vishwa Bhatt, Deasung Kim, Samrat Mukherjee, Ju-Hyung Yun, Ravi Kant Choubey, Chem. Phys. Lett., 2021, 763, 138162.
49. J. Gajendiran, S. Gnanam, V. Vijaya Kumar, K. Ramachandran, J. Ramana Ramya, S. Gokul Raj, N. Sivakumar, Chem. Phys. Lett., 2020, 754, 137639.
50. Sk. Johny Basha, V. Khidhirbrahmendra, J. Madhavi, U.S. Udayachandran Thampy, Ch. Venkata Reddy, R.V.S.S.N. Ravikumar, J. Sci.: Adv. Mater. Devices, 2019, 4, 260–266.
51. A. Garrido-Hernández, D.Y. Medina-Velazquez, A.S. de Ita y de la Torre, A. de J. Morales-Ramírez, M. Molina-Morales, M.A. Barrón-Meza, Y. Ramírez-Quirós, J. Reyes-Miranda, Mater. Sci. Semicond. Process., 2021, 121, 105403.
52. Heba Ali, Eman S. Mansor, Colloid Interface Sci. Commun., 2020, 39, 100330.
53. Felipe A. La Porta, Mateus M. Ferrer, Yuri V.B. de Santana, Cristiane W. Raubach, Valéria M. Longo, Júlio R. Sambrano, Elson Longo, Juan Andrés, Máximo S. Li, José A. Varela, J. Alloys Compd., 2013, 556, 153–159.
54. Arun Kumar, Manjeet Kumar, Vishwa Bhatt, Samrat Mukherjee, Sunil Kumar, Himanshu Sharma, M.K. Yadav, Stuti Tomar, Ju-Hyung Yun, Ravi Kant Choubey, Sens. Actuators, A, 2021, 331, 112988.

55. Chauhan NS, J. Orchid Soc. India. 1990, 4, 99–105.
56. A. Shahvar, R. Soltani, M. Saraji, M. Dinari, S. Alijani, J. Chromatogr. A. 2018, 31 (1565), 48–56.
57. Tao Chen, Wen-Qian Li, Hu. Wei-Bo, Hu. Wen-Jing, Ya.hu.A. Liu, Hui Yang, Ke Wen, RSC Adv., 2019, 9, 18008–18012.
58. Pillaiyar Puthiaraj, Su-Sung Kim, Wha-Seung Ahn, Chem. Eng. J. 2016, 283, 184–192.
59. B. Baruwati, R.S. Varma, Chem. Sus. Chem., 2009, 2, 1041–1044,
60. B. Baruwati, V. Polshettiwar, R.S. Varma, Green Chem., 2009, 11, 926–930.
61. B. Shan, Z. Yizhong, M. Sun M, Corke H., J. Agric Food Chem., 2015, 53, 7749–7759.
62. A. Szydlowska - Czerniak, R. Amarowicz, E. Szlyk, Eur. J. Lipid. Sci. Technol., 2010, 112, 750–760.
63. Pillaiyar Puthiaraj, Su-Sung Kim, Wha-Seung Ahn, Chem. Eng. J. 2016, 283, 184–192.
64. S. Dey, A. Bhunia, D. Esquivel, C. Janiak, J. Mater. Chem. A, 2016, 4, 6259–6263.
65. P. Puthiaraj, S.-M. Cho, Y.-R. Lee, W.-S. Ahn, J. Mater. Chem. A., 2015, 3, 6792–6797.
66. J. Liu, Y. Liu, X. Jiang, Y. Luo, Y. Lyu, Microporous Mesoporous Mater., 2017, 250, 203–209.
67. Kuppayee. M, Nachiyar. GKV, Ramasamy. V, Applied Surface Science, 2011, 257, 6779–6787.
68. Antoniadou. M, Daskalaki. VM, Balis. N, Kondarides. DI, Kordulis. C, Lianos. P, Applied Catalysis B: Environmental, 2011,107, 188–196.
69. J. Zhu, D. Wang, T. Liu, Ionics 2014, 20, 141.
70. M. Salavati-Niasari, D. Ghanbari, F. Davar, J. Alloys Compd. 2010, 492, 570.
71. S. Biswas, S. Kar, S. Chaudhuri, Appl. Surf. Sci. 2007, 253, 9259.
72. Ryo Inoue, Masahiko Kitagawa, Takayoshi Nishigaki, Kunio Ichino, Hiroshi Kobayashi, Masakazu Ohishi, Hiroshi Saito, J. Cryst. Growth, 1998,184–185, 1076–1080,
73. Richard Nötzel, Manfred Ramsteiner, Zhichuan Niu, Lutz Däweritz, Klaus H. Ploog, Physica E, 1998, 2, 979–982.
74. Shi, J, Chen, S, Wang, S, Ye, Z, Wu, P, Xu, G, Journal of Molecular Catalysis A: Chemical, 2019, 303, 141–147.
75. Zhang, H, Wei, B, Zhu, L, Yu, J, Sun, W & Xu, L, Appl. Surf. Sci., 2013, 270, 133–138.
76. Zhang, J, Cui, H, Wang, B, Li, C, Zhai, J, Li, Q, Chem. Eng. J., 2013, 223, 737–746.
77. Goudarzi, A, Aval, GM, Park, SS, Choi, MC, Sahraei, R, Ullah, MH, Avane, A, Ha, CS, Chem. Mater., 2009, 21, 2375–2385.
78. Yu, W, Fang, PF, Wang, SJ 2009, Appl. Surf. Sci., 2009, 255, 5709–5713.
79. Yu, X, Yu, J, Cheng, B & Huang, B, Chem. Eur. J., 2009, 15, 6731–6739.
80. J. Xu, W. Zhang, H. Fan, F. Cheng, D. Su, G. Wang, Nano Energy 2018, 51, 73–82
81. P. Zheng, Z. Dai, Y. Zhang, K. N. Dinh, Y. Zheng, H. Fan, J. Yang, R. Dangol, B. Li, Y. Zong, Q. Yan, X. Liu, Nanoscale 2017, 9, 14820–14825.
82. P. Xue, N. Wang, Y. Wang, Y. Zhang, Y. Liu, B. Tang, Z. Bai, S. Dou, Carbon 2018, 134, 222–231.

83. G.H. Yue, Y.D. Lin, X. Wen, L.S. Wang, Y.Z. Chen, D.L. Peng, Appl. Phys. A: Mater. Sci. Process. 2012, 106, 87–91.
84. C. D. Pomar, A. T. Souza, G. Sombrio, F. L. Souza, J. J. Bonvent and J. A. Souza, Chemistry Select, 2018, 3, 3774–3780.
85. K. Kalpana and V. Selvaraj, RSC Adv., 2015,5, 47766–47777
86. G.M. Xu, Y. Ma, G.J. Zhang, IEEE Trans. Plasma Sci., 2008, 36, 1352–1353.
87. Fangmin Huang, Li Chen, Honglin Wang, Zongcheng Yan, Chem. Eng. J., 2010, 162, 250–256.

Figures

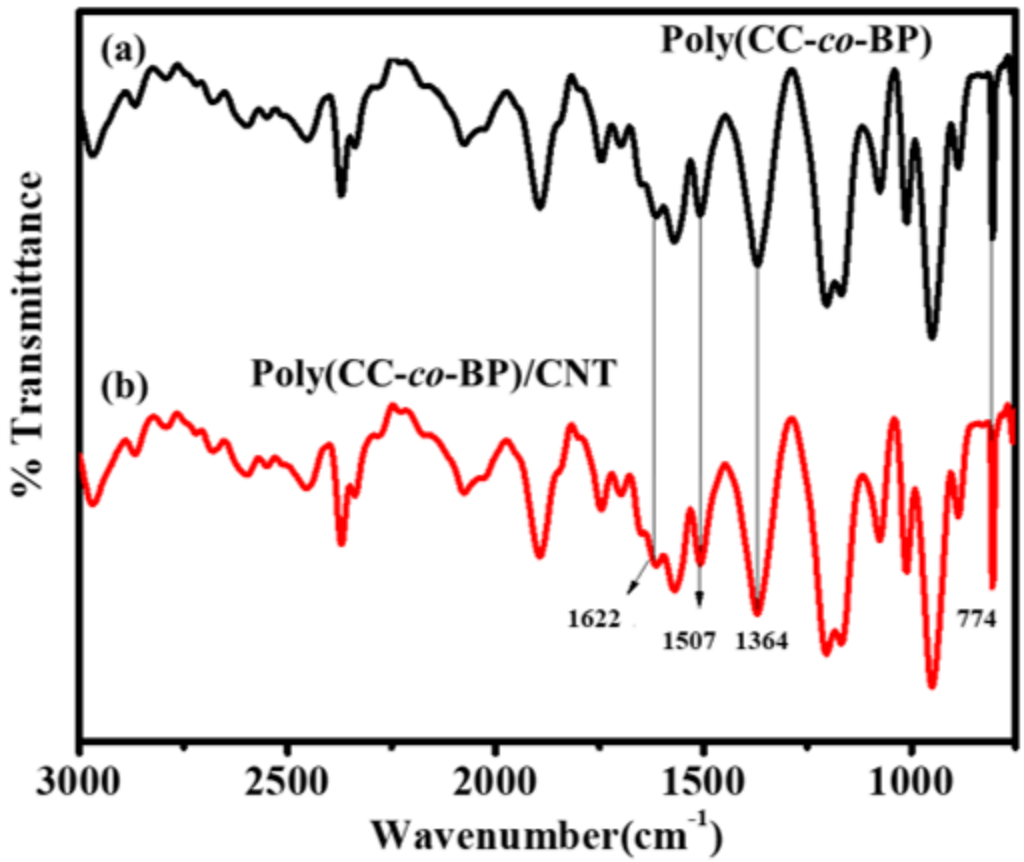

Figure 1

FT-IR spectra of (a) Poly(CC-*co*-BP) and (b) Poly(CC-*co*-BP)/CNT composite

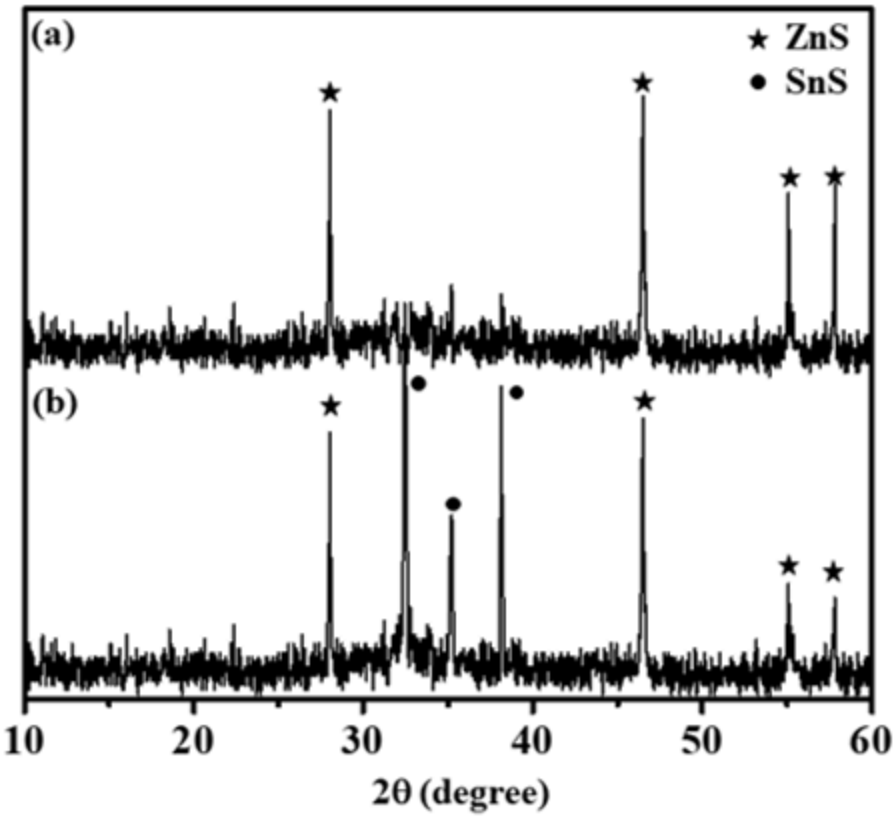

Figure 2

XRD pattern for (a) ZnS/Poly(CC-*co*-BP)-CNT and (b) ZnS-SnS/Poly(CC-*co*-BP)-CNT photocatalyst

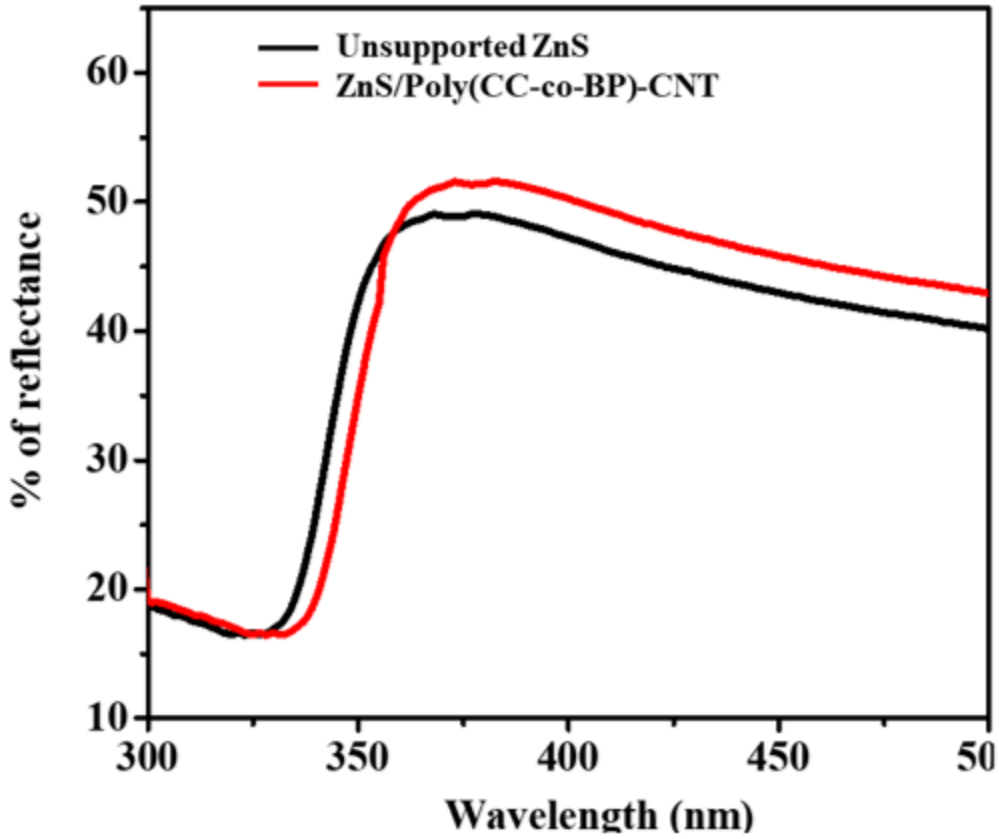

Figure 3

UV-DRS spectra of (a) unsupported ZnS and (b) ZnS/Poly(CC-*co*-BP)-CNT photocatalyst

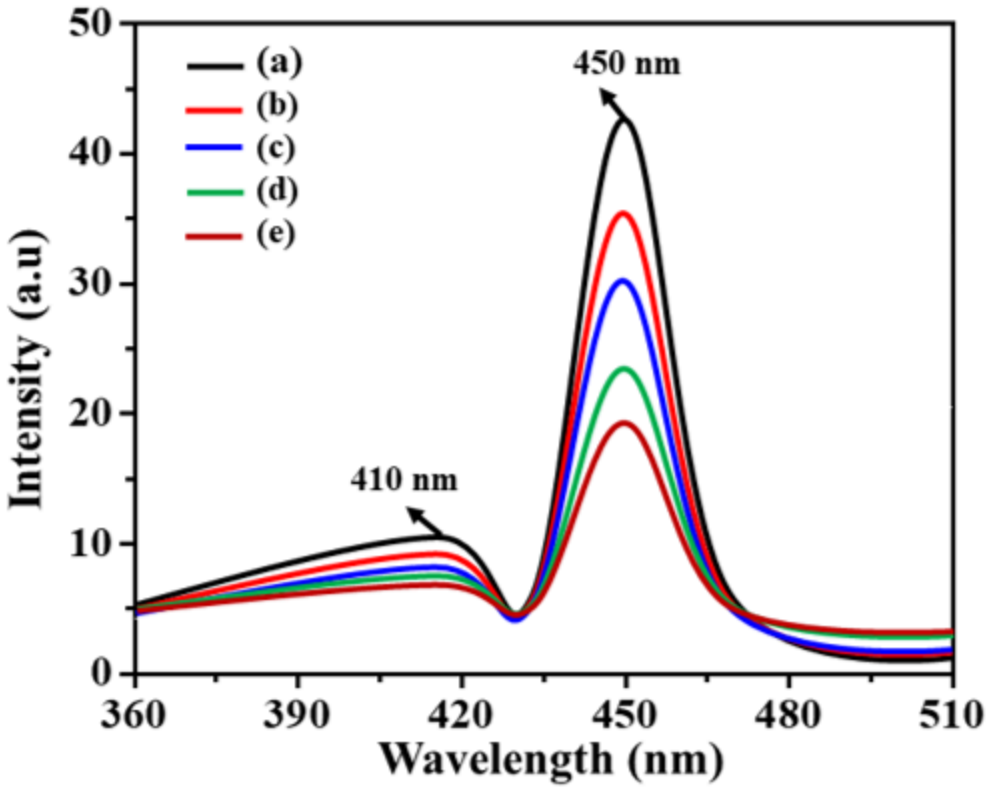

Figure 4

Photoluminescence spectra of (a) unsupported ZnS and (b) ZnS/0.25 % Poly(CC-*co*-BP)-CNT, (c) ZnS/0.5 % Poly(CC-*co*-BP)-CNT, (d) ZnS/0.75 % Poly(CC-*co*-BP)-CNT and (e) ZnS/1% Poly(CC-*co*-BP)-CNT photocatalyst

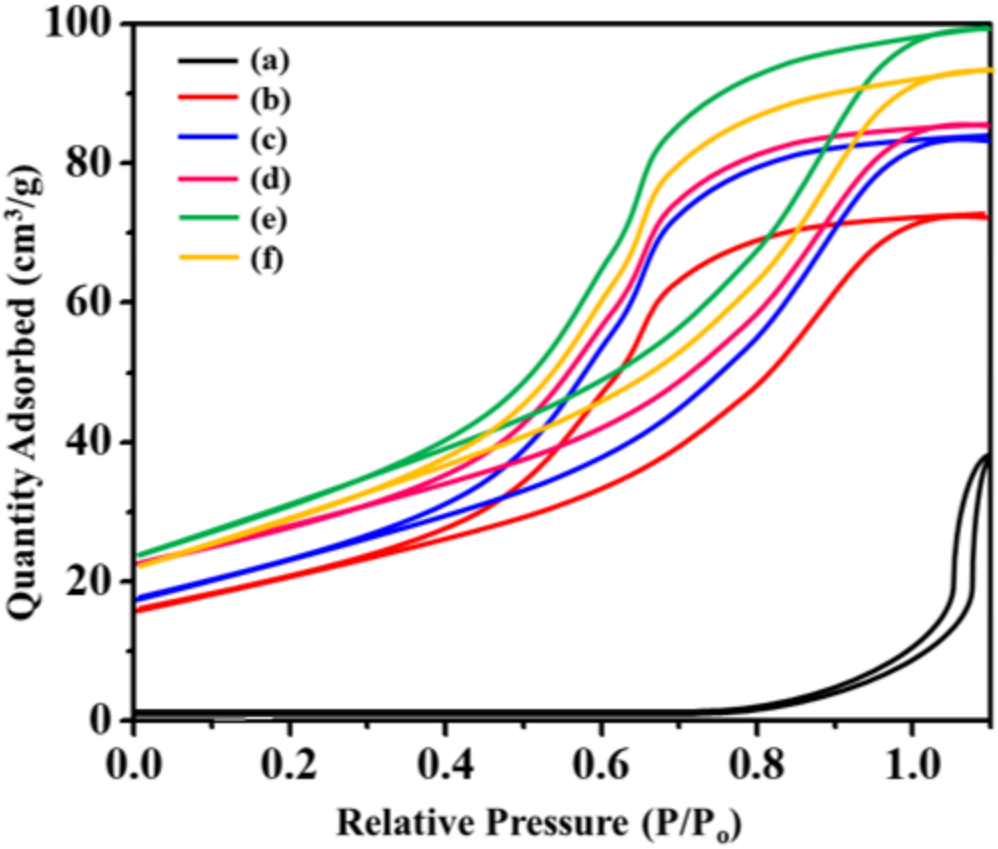

Figure 5

Nitrogen adsorption-desorption isotherm of (a) Poly(CC-*co*-BP)-CNT composite, (b) unsupported ZnS (c) ZnS/0.25% Poly(CC-*co*-BP)-CNT, (d) ZnS/0.5% Poly(CC-*co*-BP)-CNT and (e) ZnS/1%Poly(CC-*co*-BP)-CNT and (f) ZnS/1.25% Poly(CC-*co*-BP)-CNT photocatalyst

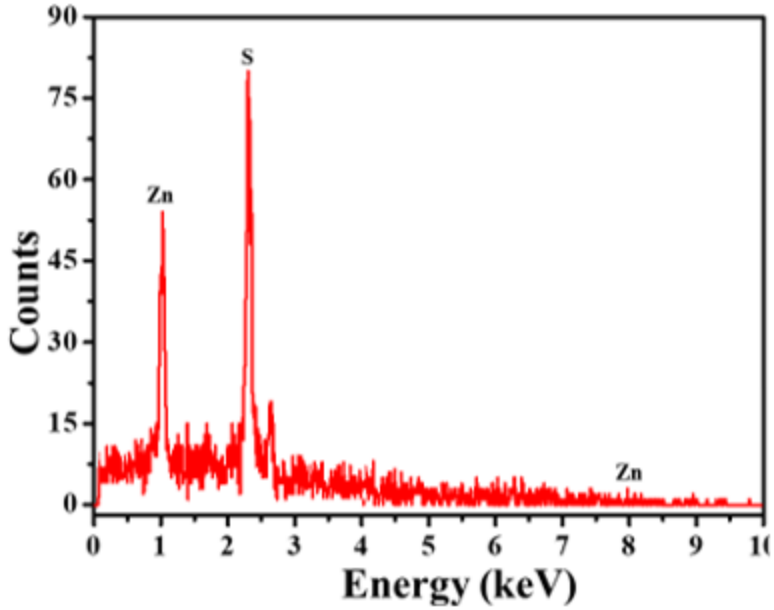

Figure 6

EDX spectra of ZnS/Poly(CC-*co*-BP)-CNT photocatalyst

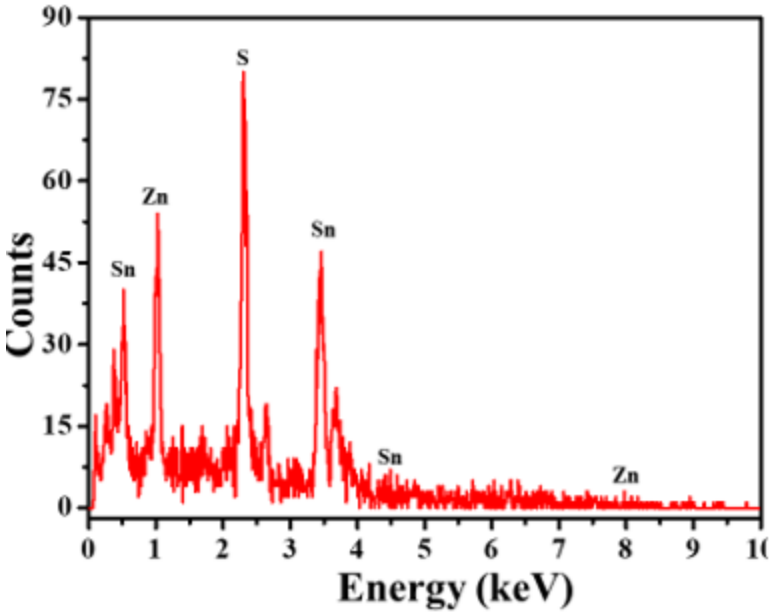

Figure 7

EDX spectra of ZnS-SnS/Poly(CC-*co*-BP)-CNT photocatalyst

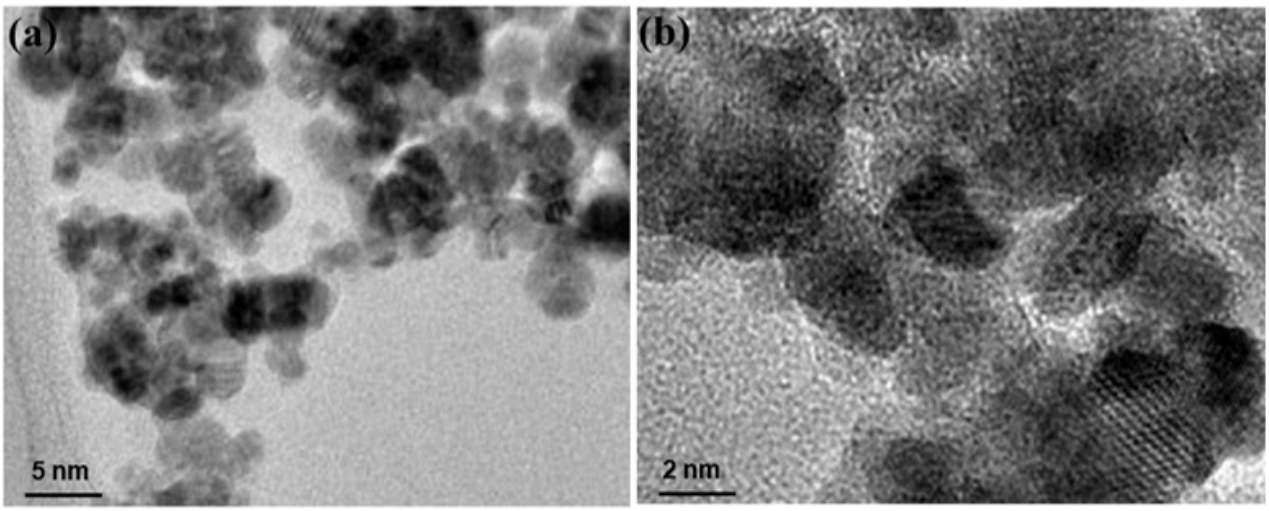

Figure 8

HR-TEM image of (a) ZnS/Poly(CC-*co*-BP)-CNT and (b) ZnS-SnS/Poly(CC-*co*-BP)-CNT photocatalyst.

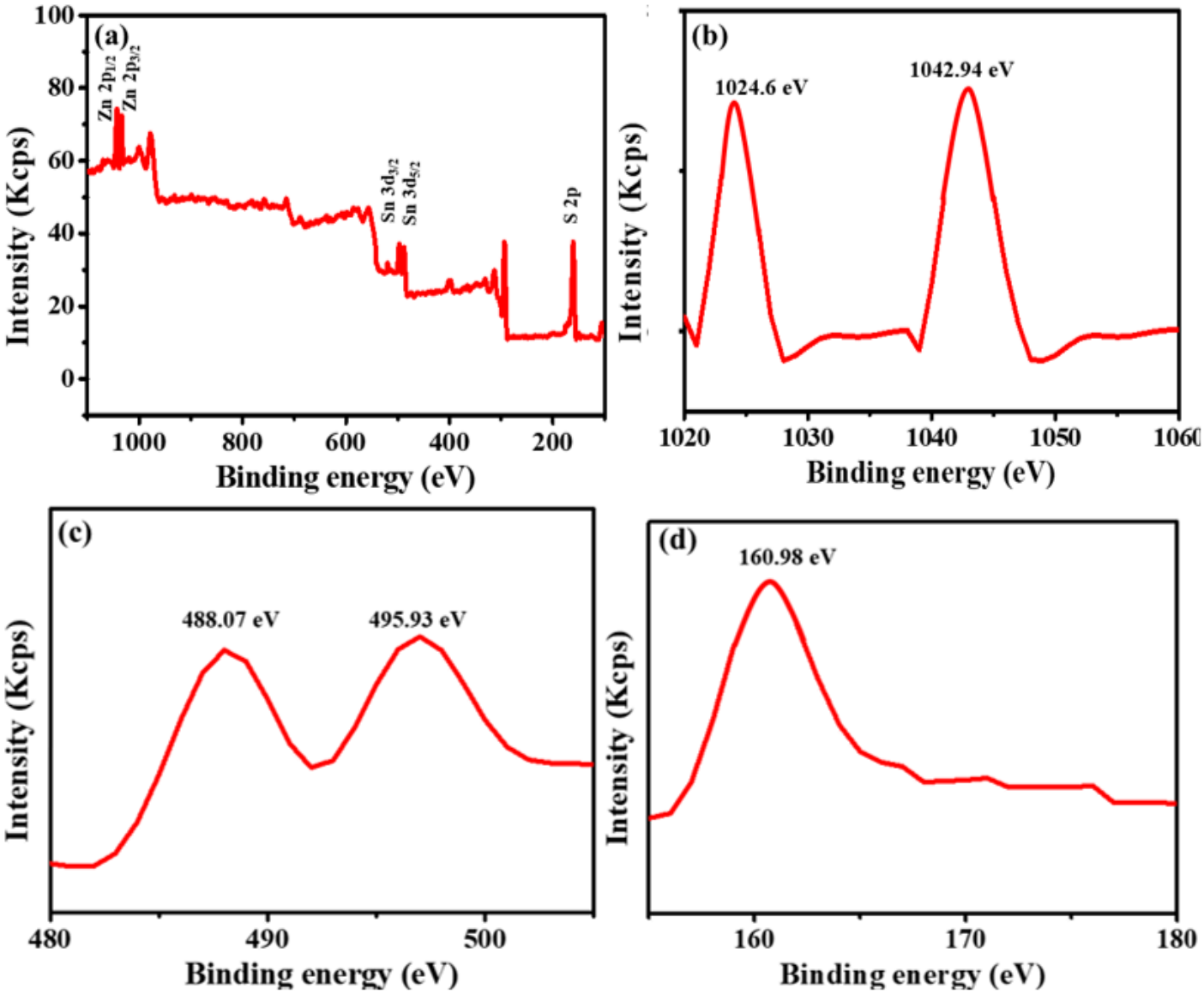

Figure 9

(a) XPS full scan spectrum of ZnS-SnS/Poly(CC-*co*-BP)-CNT and XPS spectra of (b) Zn 2p peak (c) Sn 3d peak and (d) S 2p peak in ZnS-SnS/Poly(CC-*co*-BP)-CNT photocatalyst.

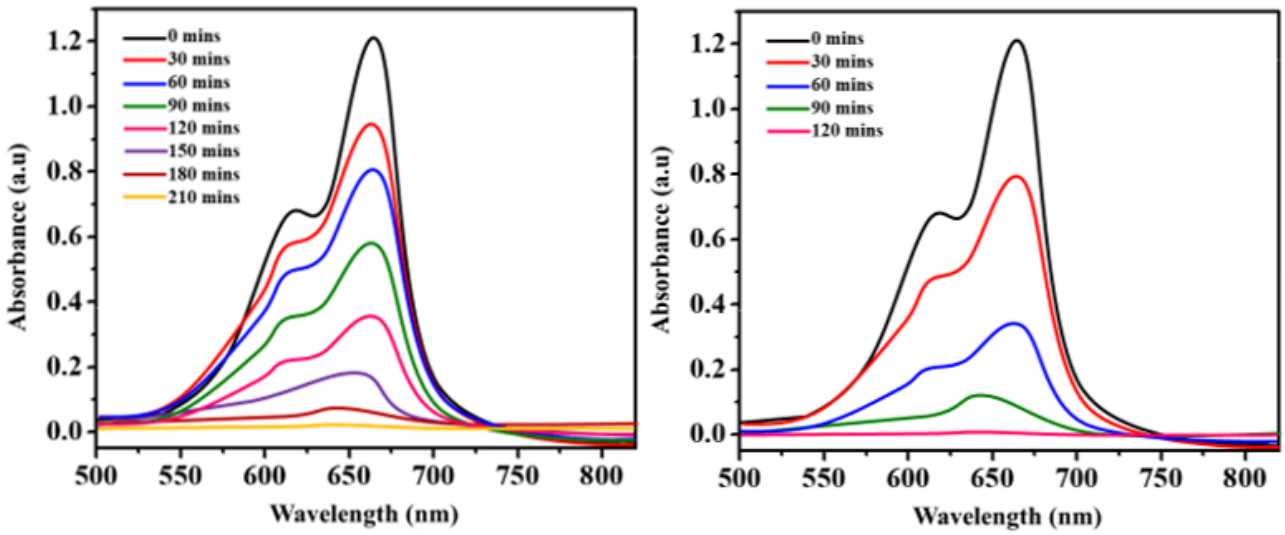

Figure 10

Time dependence UV visible spectra of methylene blue dye (12 ppm) using unsupported ZnS (50 mg) photocatalyst under (a) Natural sun light (b) UV3 irradiation

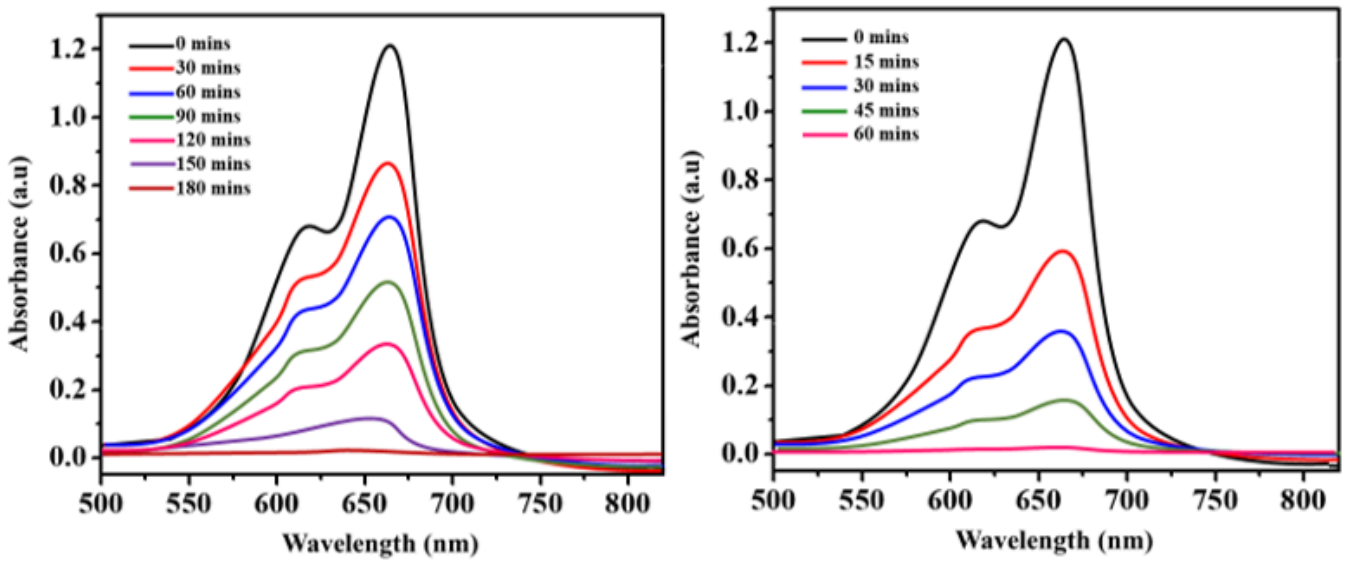

Figure 11

Time dependence UV visible spectra of methylene blue dye (12 ppm) using ZnS/1% Poly(CC-*co*-BP)-CNT (50 mg) photocatalyst under (a) Natural sun light (b) UV3 irradiation

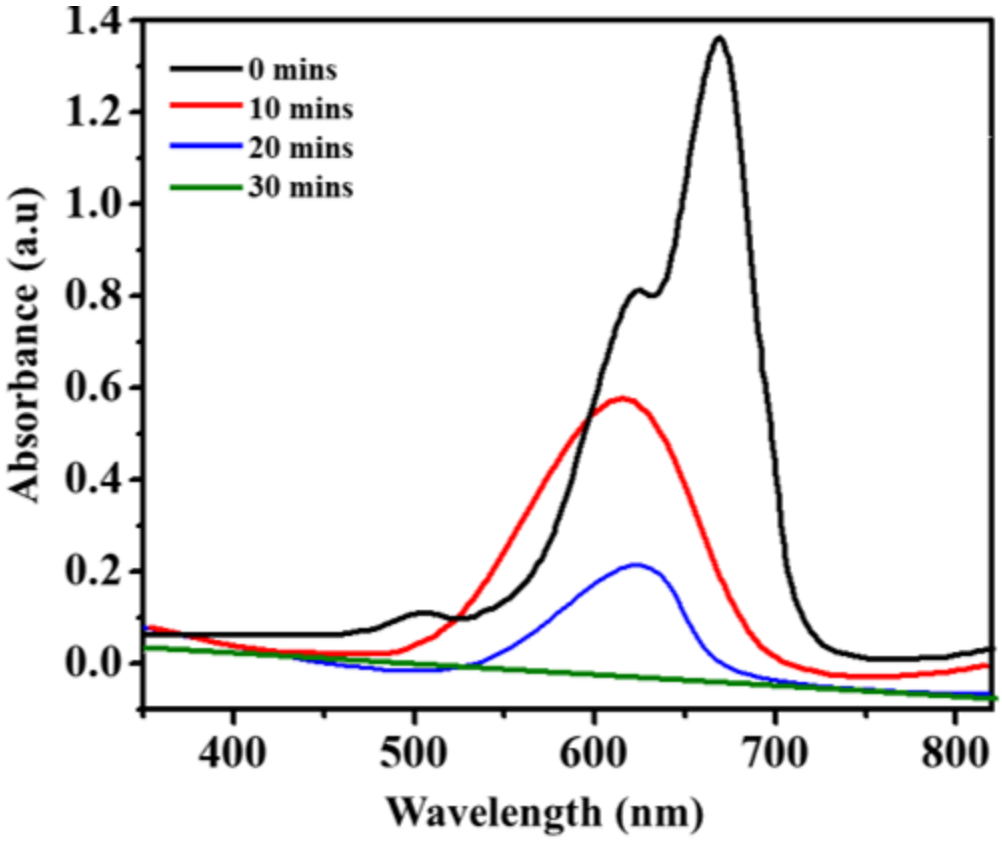

Figure 12

Time dependence UV visible spectra of methylene blue dye (12 ppm) using $ZnS^{1}SnS^{1}$/1% Poly(CC-*co*-BP)-CNT (50 mg) photocatalyst under UV3 irradiation.

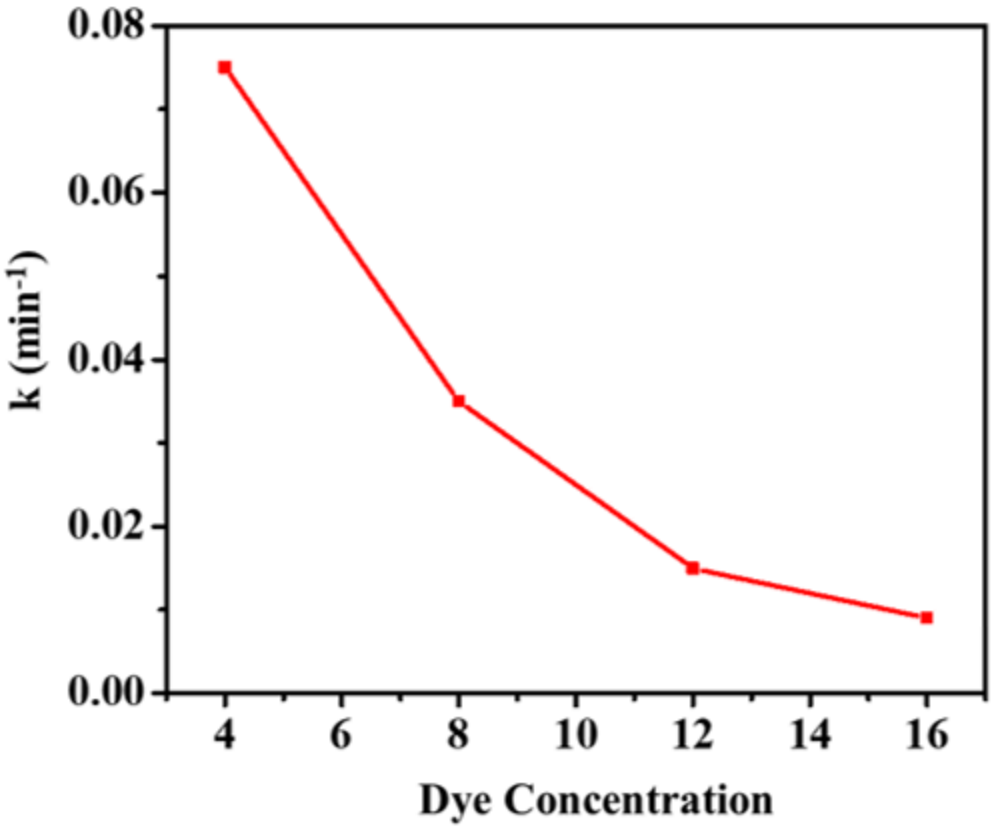

Figure 13

Effect of methylene blue dye concentration versus rate of MB dye degradation for $ZnS^{1}SnS^{1}$/1%Poly(CC-*co*-BP)-CNT photocatalyst

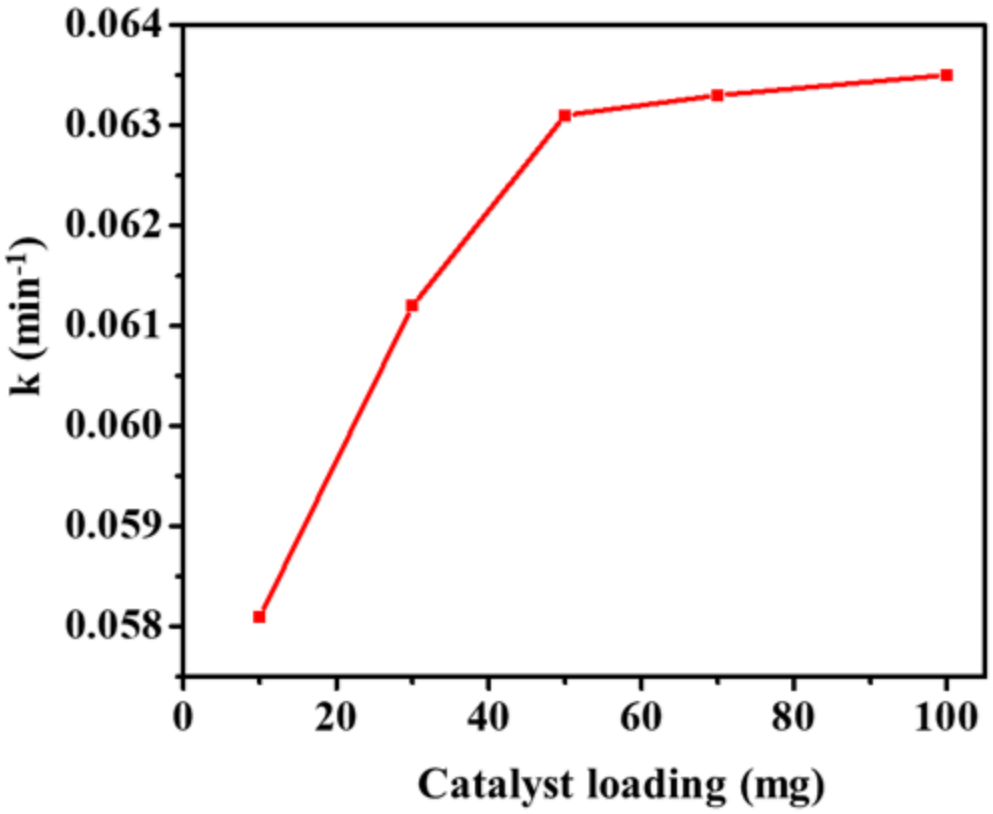

Figure 14

Effect of photocatalyst weight (MB=12ppm) versus rate of MB dye degradation and for $ZnS^{1}SnS^{1}$/1%Poly(CC-*co*-BP)-CNT photocatalyst.

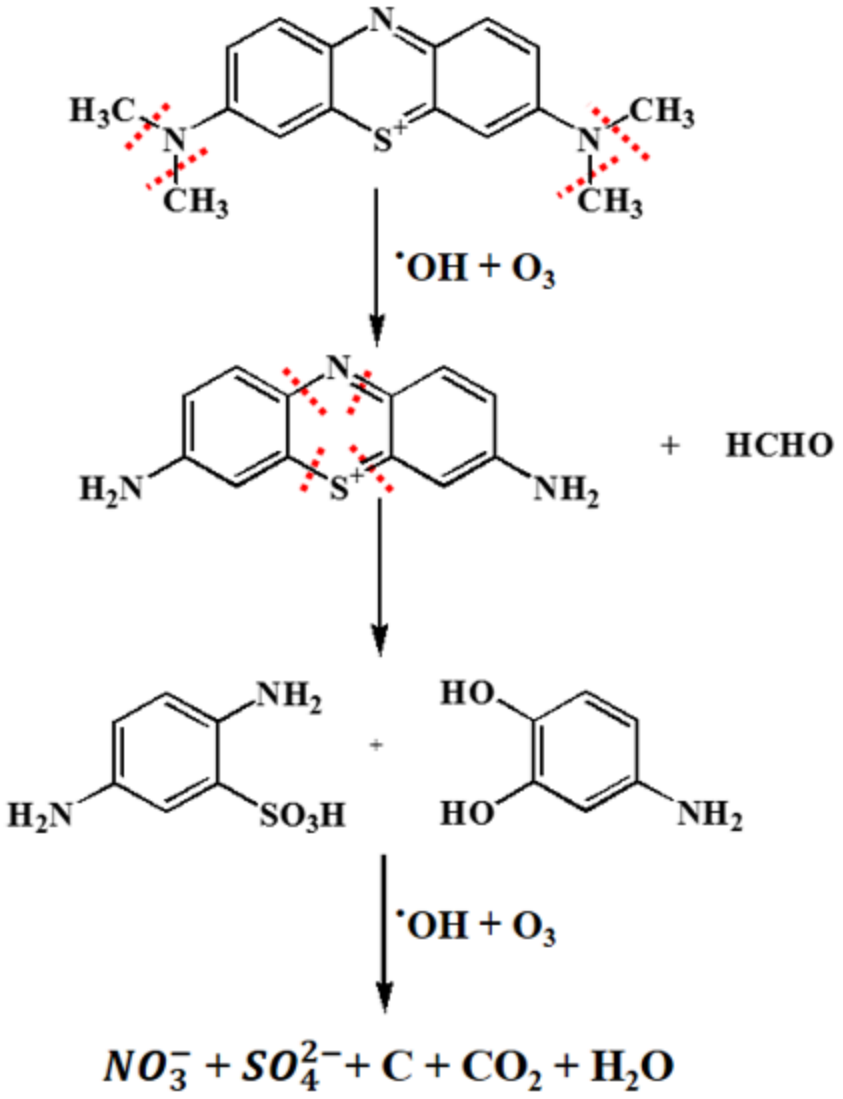

Figure 15

Proposed mechanism for the methylene blue dye degradation using ZnS[1]SnS[1]/1%Poly(CC-*co*-BP)-CNT photocatalyst in UV irradiation.

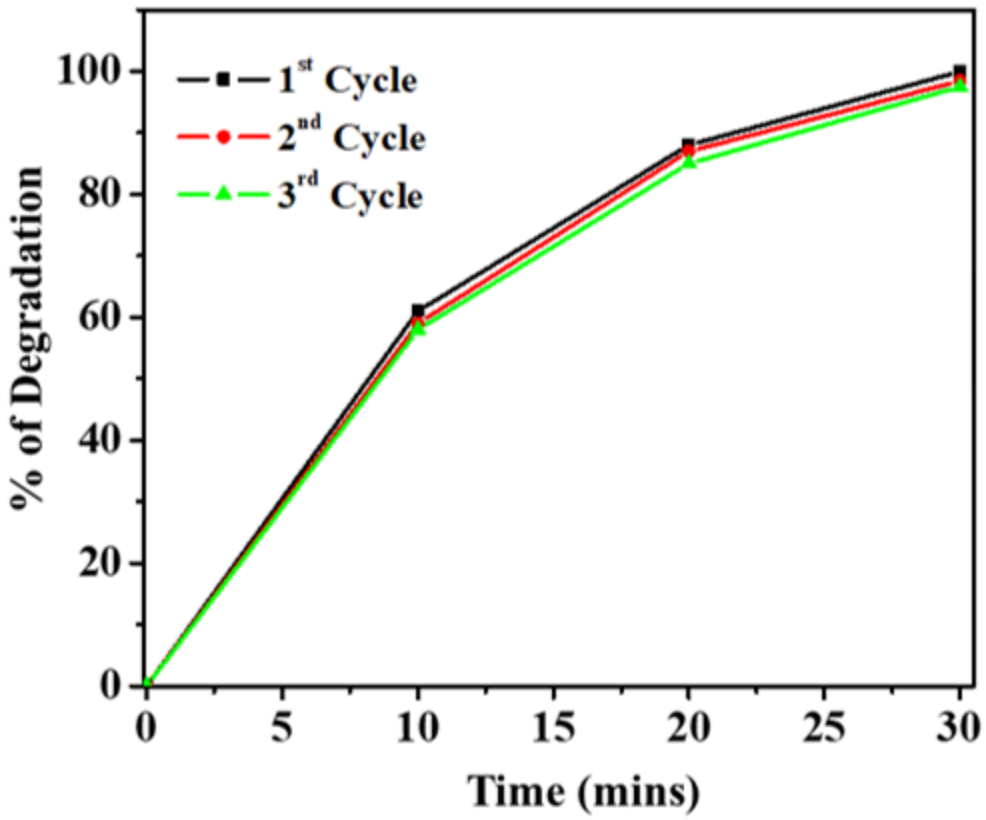

Figure 16

Reusability of ZnS[1]SnS[1]/1%Poly(CC-*co*-BP)-CNT photocatalyst for methylene blue dye degradation under UV3 irradiation